JOURNAL OF AIRCRAFT
Vol. 44, No. 2, March–April 2007

Structures of the Low-Altitude Stationary Flight Test Vehicle

Shoji Maekawa* and Masaaki Nakadate†
Japan Aerospace Exploration Agency, Mitaka, Tokyo 181-0015, Japan
and
Atsushi Takegaki‡
Fuji Heavy Industries, Ltd., Utunomiya, Tochigi 320-8564, Japan

DOI: 10.2514/1.25044

Between March and November 2004, the flight tests of the low-altitude stationary flight test vehicle were successfully conducted at Taiki-cho, Hokkaido, Japan. The objectives of these flight tests were to study structural feasibility, as well as control and operational methods, for a stratospheric platform. The structures of this airship are briefly outlined. This airship employed new envelope materials developed for the stratospheric platform. The development test data, as well as deterioration test data of these materials, are shown. The design loads are compared with the flight test results. Some considerations are given to ballonet sloshing.

Nomenclature

a = longitudinal dimension of a rectangle
d = diameter of a cylinder
g = gravitational acceleration
h = depth of the air in the ballonet
L = half of an ellipsoid height
N_x = longitudinal load factor
N_y = lateral load factor
N_z = vertical load factor
R = radius of an ellipsoid

I. Introduction

BETWEEN March and November 2004, the flight tests of the low-altitude stationary flight test vehicle [1] were conducted at Taiki-cho, Hokkaido, Japan. The objectives of the flight tests were to study structural feasibility, as well as control and operational methods [2,3], for a stratospheric platform. The target of this unmanned flight test vehicle was to stay within a small space at the altitude of 4 km. The autonomous control was adopted for high-altitude flight, though human remote control was maintained for takeoff and landing, as well as for emergency measures. For this purpose, a blimp with the overall length of 68.4 m was developed. To make the pressure height more than 4 km, the total size of its ballonets were made to be 50% of the envelope volume. To simulate the stratospheric platform, the propulsion system adopted electrical motors to drive two ducted propellers, and turboshaft engines are used for generation of electricity. Nine flight tests were conducted. The first two flights in the first-stage flight test were tethered takeoffs and landings. Four flights were performed in the second-stage flight test to study the airship characteristics flying below the altitude of 600 m. Three flights were conducted in the third-stage flight test. The airship flew at high altitude no more than 4 km and performed stationary flights. The flight test included successful stationary flights at the altitude of 4 km, under both autonomous control and human remote control. Figure 1 shows the blimp flying at the altitude of 4 km.

Presented as Paper 7407 at the AIAA 5th Aviation, Technology, Integration, and Operations Conference, Arlington, VA; received 16 May 2006; revision received 25 May 2006; accepted for publication 10 October 2006.

*Senior Researcher, Unmanned and Innovative Aircraft Team, 6-13-1 Osawa. Member AIAA.
†Section Leader, Unmanned and Innovative Aircraft Team, 6-13-1 Osawa. Member AIAA.
‡Senior Engineer, Engineering and Development Center, 1-1-11 Yonan.

II. Stationary Flight Test Vehicle

In the process of the stratospheric platform development, two flight test vehicles were developed: the ground-to-stratosphere flight test vehicle and the low-altitude stationary flight test vehicle. The former flew in August 2003 at Hitachi, Ibaragi, Japan [4]. It has reached the altitude of 16.4 km (Fig. 2).

The low-altitude stationary flight test vehicle was aimed to fly and stay in a small space at the altitude of 4 km to study control and operational feasibility, as well as structural integrity. This airship equips electrical motors for driving ducted propellers and turboshaft engines to generate electricity. Unmanned control is a presupposition and autonomous control is adopted for normal flight, and human remote control is for takeoff and landing, as well as for emergency measures. The size of the blimp is 68.4 m in length 17.5 m in width, and 21.1 m in height. The volume of the envelope is 10, 660 m^3 and the net mass is 6400 kg (Fig. 3).

III. Outline of the Structures

The structures of this airship are rather conventional as a blimp. Major features of its structures are briefly described in the following sections.

A. Envelope and Ballonet

The envelope has an overall length of 67.8 m and the maximum diameter of 17.5 m. The fineness ratio is 3.87. The envelope has a volume of 10, 660 m^3. Inside the envelope there are three ballonets. The fore ballonet has a volume of 1790 m^3, which is 17% of the envelope volume. The mid ballonet volume is 1050 m^3 and 10% of the envelope. Those of the aft ballonet are 2420 m^3 and 23%, respectively. The mid ballonet is mainly for pressure control, and the other two are for both pressure and pitch control.

The envelope is made of Vectran, which will be described in detail in the next section, whereas the ballonet material is Power Rip. The latter is layered with Eval and protected by polyurethane at both sides. The thickness is 0.099 mm and the density is 100 g/m^2.

B. Tail Surfaces

The cross-shaped tail surfaces are made of aluminum spars and ribs covered with films (Fig. 4). The total area of the horizontal tails is 64.4 m^2 and that of the vertical tails is 75.6 m^2. The total area of the elevators is 9.1 m^2 and that of the rudders is 10.8 m^2. The upper vertical surface is covered with Zylon, whereas the other surfaces are covered with Power Rip. Zylon is applied to study its durability

Fig. 1 Stationary flight test vehicle.

Fig. 2 The ground-to-stratosphere flight test (a picture taken from the vehicle).

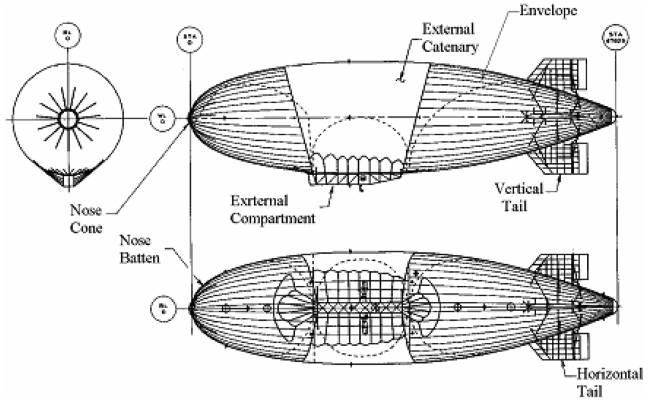

Fig. 3 Three-view drawing.

during the flight tests. The elevators and the rudders are also made of Zylon and Power Rip, and they are driven by electric actuators.

The Power Rip used for the tail surfaces is layered with polyurethane, which is faced outside. The thickness is 0.14 mm and the density is 90 g/m^2.

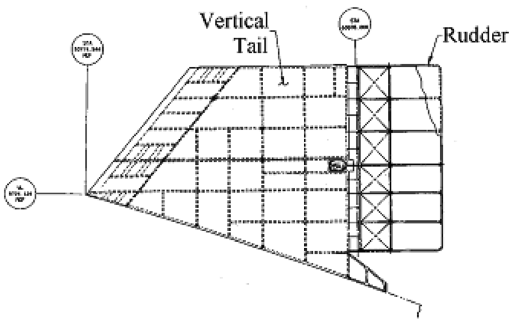

Fig. 4 Vertical tail.

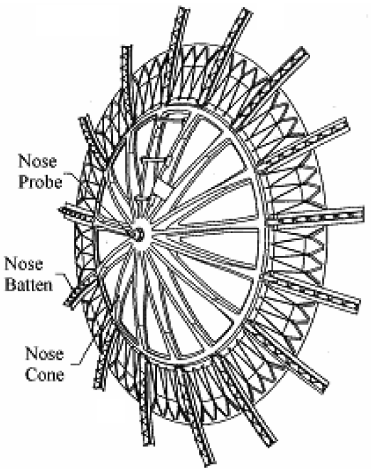

Fig. 5 Nose cone and nose battens.

C. Nose Cone and Nose Battens

The nose of the envelope is strengthened by a nose cone and nose battens, which are made of glass-fiber-reinforced plastics (Fig. 5). The length of the nose battens is about 8% of the airship length.

D. External Compartment

The external compartment, made of aluminum frames and honeycomb panels, is hung under the envelope (Fig. 6). The honeycomb panels for mid and aft bays are made of aluminum alloys, although those for the two fore bays are made of glass-fiber-reinforced plastics. It is for radio wave penetration, which is required for mission systems in the early design phase. Later, this requirement became obsolete and metal mesh sheets were installed inside the mission bay panels to avoid electromagnetic interference. The flight control systems were installed inside the compartment. Two turboshaft engines, Rolls Royce 250-C20W, are also installed inside

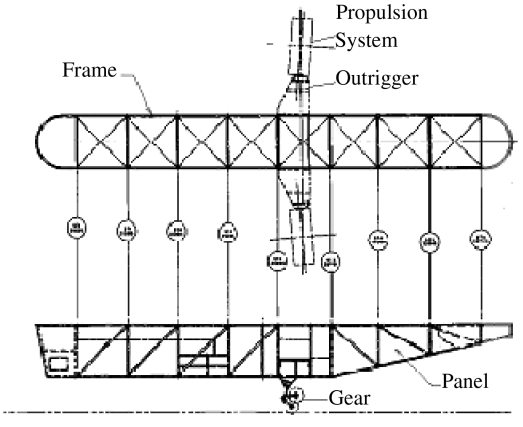

Fig. 6 External compartment.

the compartment with ac and dc generators. A fuel tank and a water ballast tank are also equipped.

The external compartment is hung under the envelope with external catenaries made of Vectran. This system was selected to avoid the interference with ballonets.

E. Propulsion System

The outriggers were protruded from both sides of the external compartment, to carry motor-driven ducted propellers. The motors are Pacific Powertec E213G4 and the propellers are MT-Propeller MTV-7-D-R/152-23. These propulsion systems can tilt upward to 120 deg and downward to −90 deg.

F. Landing Gear

The single fixed gear was installed underneath the compartment. This wheel unit can swivel through 360 deg.

IV. Envelope Materials

This blimp has employed new envelope materials, Vectran and Zylon, which have been developed for the stratospheric platform system [5,6]. Vectran is made of polyarylate (PA) fibers and is a product of Kuraray Co., Ltd. Zylon is made of poly-paraphenylene benzobisoxazole (PBO) fibers and is a trademark of Toyobo Co., Ltd. Their strength has been much improved from current polyester-based envelope materials. They were applied to the envelope and the tail surface. These materials have also been installed on the top of the envelope, for deterioration monitoring. They were partially cut off and tested in October 2004. The layer compositions of Vectran and Zylon are shown in Figs. 7 and 8. Normally, Zylon is layered with aluminum-evaporated Tedlar to protect against weathering, which shows good antiweathering properties. However, this layer composition was chosen for the stationary flight test vehicle and its accelerated environmental test results were not satisfactory.

A. Mechanical Properties of the Materials

In the early stage of the development, the material development test was conducted. Twelve mechanical properties, as well as physical and environmental properties, were measured in this test. Measured mechanical properties are tensile strength, joint tensile strength, fatigue strength, joint fatigue strength, creep strength, joint creep strength, bending strength, joint bending strength, wear resistance, biaxial tensile strength, crack resistance, and inplane shear strength.

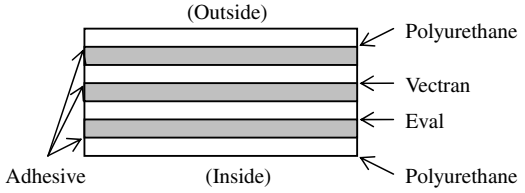

Fig. 7 Layer composition of Vectran.

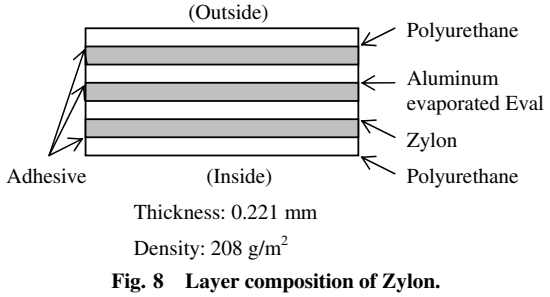

Fig. 8 Layer composition of Zylon.

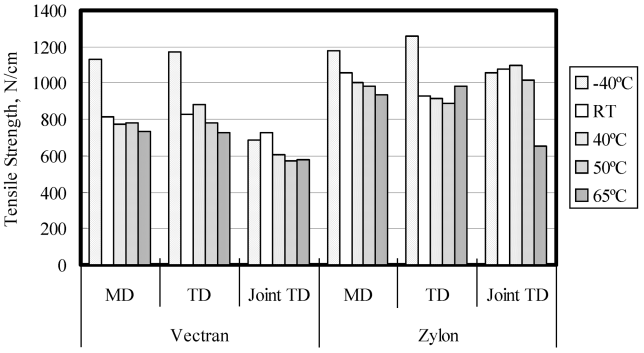

Fig. 9 Tensile properties.

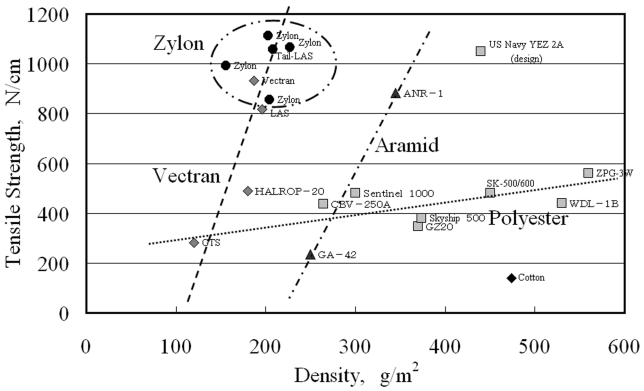

Fig. 10 Comparison of envelope materials.

Figure 9 shows the tensile properties of Vectran and Zylon in the machine direction (MD) and the transverse direction (TD), as well as those of the joint section of these materials in the transverse direction. The environmental temperature is varied between −40 and 65°C. Both materials satisfied the strength requirement of 686 N/cm (70 kgf/cm) at room temperature, specified for the stationary flight test vehicle.

Figure 10 shows a comparison of the tensile properties of various envelope materials. Vectran and Zylon show very high specific strength.

Table 1 shows the creep strength of the joint section in the transverse direction. Both materials show good creep resistance at room temperature, though at high temperatures, their creep strength decreases.

B. Physical Properties

Measured physical properties are weight, specific heat, thermal conductivity, solar absorptance, thermal emittance, helium gas permeability, surface and volume electric resistance, dielectric constant, and dielectric loss. All the tests were conducted for Vectran, but only weight test and permeability test were conducted for Zylon.

Measured weight and thickness of Vectran and Zylon are shown in Figs. 7 and 8.

Table 1 Creep strength of joint section

Vectran	RT	137 N/cm	No failure after 300 h
	50°C	137 N/cm	No failure after 300 h
	65°C	69 N/cm	No failure after 300 h
	65°C	137 N/cm	Failed after 5.8, 13.6, and 13.6 h
Zylon	RT	137 N/cm	No failure after 300 h
	50°C	69 N/cm	No failure after 300 h
	50°C	137 N/cm	Failed after 2.7, 3.3, and 3.7 h
	65°C	69 N/cm	No failure after 300 h
	65°C	137 N/cm	Failed after 0.3, 0.4, and 1.5 h

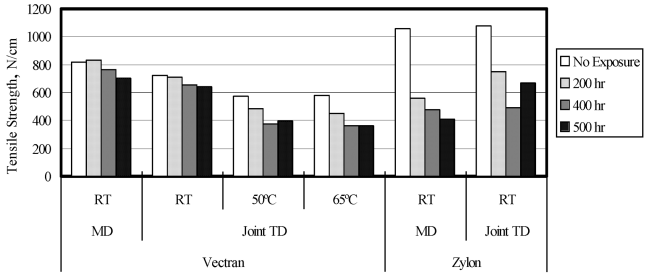

Fig. 11 Tensile strength after xenon exposure.

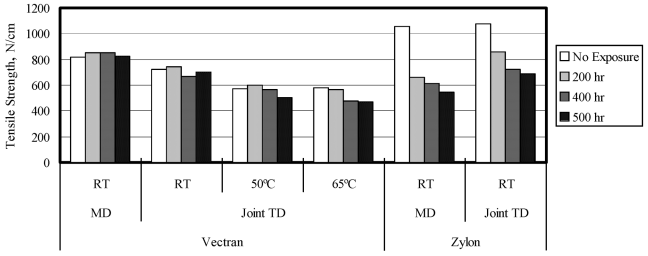

Fig. 12 Tensile strength after sunshine exposure.

C. Environmental Properties

For the environmental properties, accelerated exposure tests were conducted in a xenon weatherometer and a sunshine weatherometer. Moisture tests, ozone exposure tests, and outdoor exposure tests were also carried out. All of these tests were conducted for Vectran, but only the accelerated exposure tests were performed for Zylon.

Figure 11 shows the tensile strength of Vectran and Zylon after accelerated exposure in the xenon weatherometer, with radiant energy of 180 W/m^2. Figure 12 shows the tensile strength after exposure in the sunshine weatherometer, with radiant energy of 255 W/m^2. The xenon chamber simulates the sunlight spectrum, and the sunshine chamber simulates ultraviolet exposure.

D. Deterioration Test

All of the envelope materials (i.e., Vectran, Zylon, and Power Rip) have been installed on the top of the envelope for deterioration monitoring. They were partially cut off and tensile-tested in October 2004. As shown in Table 2, Vectran and Zylon retained enough strength.

Table 2 Tensile strength after flight tests

		Development test, N/cm	Deterioration test, N/cm	Retention ratio, %
Vectran		817	722	88
Vectran-joint		726	829	114
Zylon		1057	1038	98
Power Rip	Ballonet	77	70	91
	Tail	114	97	85

V. Loads

A. Flight Load

The maneuver, gust, and ground loads were estimated following the conditions specified in FAA-P-8110-2 "Airship Design Criteria" [7], in which sixteen cases of maneuver loads are specified. Table 3 shows the cases that resulted in larger design load factors, which include the descent and pull-up case that gives the maximum vertical load factor, $N_z = 1.14\ g$. The nose-up and nose-down cases give the maximum and minimum longitudinal load factors, $N_x = \pm 0.5\ g$. The turn-and-dive case gives the maximum and minimum lateral load factors, $N_y = \pm 0.12\ g$.

Twenty cases are calculated for the gust loads. Static heaviness, airship velocity, gust velocity, gust directions, flight control conditions, and gust length are varied in the calculations. Table 4 shows the cases for the maximum and minimum load factors. The minimum and maximum gust loads are $N_x = -0.05$ and $0.12\ g$, $N_y = \pm 0.78\ g$, and $N_z = 0.24$ and $1.71\ g$. For this airship, the gust load is dominant in the lateral and vertical directions.

The minimum and maximum measured data are $N_x = -0.31$ and $0.37\ g$, $N_y = -0.02$ and $0.03\ g$, and $N_z = 0.92$ and $1.04\ g$, as shown in Table 5. A specific flight test for load factor measurement was not conducted, but the data were measured during the normal flights. The measured data are within the estimated load factors. The discrepancy was caused because the flight was limited to low-wind conditions, and so the severe gust was not encountered.

B. Ground Load

The ground loads are calculated following airship design criteria. The design landing load is given as $0.69\ g$, whereas the energy-absorption test of the landing gear shows $0.56\ g$. The descent velocity is assumed to be 0.914 m/s (3 ft/s) and the landing mass is 6550 kg. The maximum measured load is 16,300 N, which is about one-third of the design load factor.

Table 3 Design maneuver loads

Condition	Speed, m/s	Mass, kg	Attitude	Thrust direction	Control surface position			Peak acceleration		
					Rudder	Elevator		Nx, g	Ny, g	Nz, g
Level flight	15	6550	+3.7 deg	Forward	Neutral	Neutral	-	0.06	0.00	1.00
Nose-down	15	6400	+30 deg	Forward	Neutral	-	-	**−0.50**	0.00	**0.87**
Nose-up	15	6400	−30 deg	-	Neutral	-	-	**0.50**	0.00	**0.87**
Descent and pull-up	15	6550	−41 deg + 9 deg	Forward	Neutral	Full down	Min	−0.01	±0.00	0.89
						Full up	Max	0.05		**1.14**
Turn and dive	15	6400	Horizontal	Forward	Full over	Full down	Min	−0.01	**±0.12**	0.95
							Max	0.04		1.05

Table 4 Design gust loads

Condition	Speed, m/s	Gust vel., m/s	Gust direction	Control	Control surface position		Gust length	Peak acceleration			
					Rudder	Elevator			Nx, g	Ny, g	Nz, g
Level flight (max. lightness)	9.75	10.5	Vertical (down)	No control	Neutral	Neutral	Min	Min	0.00	±0.00	**0.24**
								Max	**0.12**		1.15
Level flight (max. lightness)	9.75	10.5	Vertical (up)	No control	Neutral	Neutral	Min	Min	−0.01	±0.00	0.81
								Max	0.04		**1.71**
Level flight (max. lightness)	9.75	10.5	Lateral	No control	Neutral	Neutral	Min	Min	−0.01	**±0.78**	0.88
								Max	0.06		1.02

Table 5 Flight test results

Direction	Flight test result, g		Design maneuver load factor, g		Design gust load factor, g	
	Max.	Min.	Max.	Min.	Max.	Min.
x	0.37	−0.31	0.5	−0.5	0.12	−0.05
y	0.03	−0.02	0.12	−0.12	0.78	−0.78
z	1.04	0.92	1.14	0.87	1.71	0.24

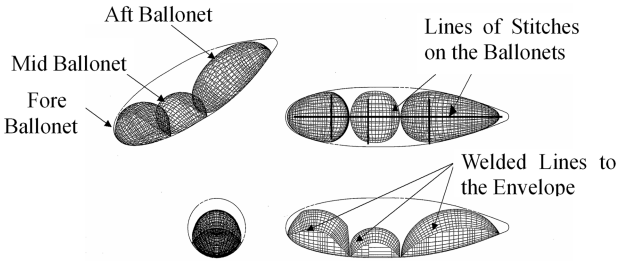

Fig. 13 Ballonets.

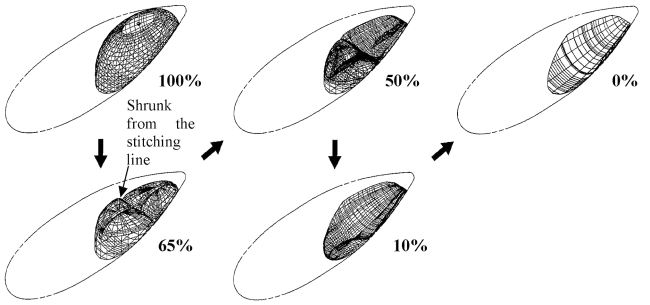

Fig. 14 Contraction of the aft ballonet.

Among the mooring and handling loads, the mast handling-override load is chosen here to compare the design value with the measured data. The design mast reaction load is 55,900 N for this case, and the maximum measured longitudinal load factor is 0.324 g. This corresponds to the mast reaction load of 44,800 N, which is about 80% of the design value. The override velocity, 1.54 m/s (3 kt), specified in "Airship Design Criteria" gives good estimation.

VI. Ballonet Sloshing

For buoyancy and trim control, this blimp has three ballonets inside the envelope. To make the pressure height more than 4 km, the total size of the ballonets is made to be 50% of the envelope volume. Figure 13 shows the shape of the ballonets when they are full. Because the sizes of the ballonets are big, ballonet sloshing was a concern [8,9]. However, no sloshing problem occurred during the flight tests.

Figure 14 shows the configuration change of the aft ballonet when its volume decreases. The ballonet uses the envelope as a bottom surface, so that it leans forward and the bottom surface is U-shaped. Such a shape makes the inside air stable around the bottom, because of the gravity. In addition, it is stitched as shown by the arrow in Fig. 14, so that it sinks from the stitched lines when the volume decreases. Thus, the length of the ballonet shortens when the volume decreases.

If the ballonet is assumed to keep its configuration, the fundamental frequency ω_1 of ballonet sloshing can be obtained for some simplified ballonet configurations :

$$\omega_1^2 = \frac{\pi g}{a}\tanh\frac{\pi h}{a}$$

for a rectangular configuration, and

$$\omega_1^2 = \frac{3.68g}{d}\tanh\frac{3.68h}{d}$$

for a cylindrical ballonet, and

$$\omega_1^2 = \frac{g}{R}\lambda_1$$

for an ellipsoidal ballonet, where λ_1 is a function of L/R and h/L.

The frequency of sloshing is governed by the length of the ballonet, so that it becomes higher as the ballonet length decreases. Therefore, the interference with the airship characteristic frequency, which is usually lower than the sloshing frequency, decreases.

The same argument can be applied to the fore ballonet. The center ballonet is put between the fore and aft ballonets and the movement is constrained. Thus, ballonet sloshing can be avoided by adequate shape selection, as long as the size of the ballonets is small.

VII. Conclusions

A wide range of knowledge on the airship structures has been obtained through the development and flight tests of the low-altitude stationary flight test vehicle. The merits and demerits of nonrigid airship structures have been learned, and this knowledge should be applied to the development of the stratospheric platform. The style of the structures should be examined from the beginning, because the size of the airship will be completely different.

References

[1] Nakadate, M., "Flight Test Overview of Low Altitude Stationary Flight Test Vehicle," *The Fifth Stratospheric Platform Systems Workshop Proceedings*, SPSW2005 Program Committee, Tokyo, Japan, 2005, pp. 129–136.

[2] Kohno, T., "Flight Control of Low Altitude Stationary Flight Test Vehicle," *The Fifth Stratospheric Platform Systems Workshop Proceedings*, SPSW2005 Program Committee, Tokyo, Japan, 2005, pp. 143–150.

[3] Harada, K., "Buoyancy Control of Ground to Stratosphere/Low Altitude Stationary Flight Test Vehicles," *The Fifth Stratospheric Platform Systems Workshop Proceedings*, SPSW2005 Program Committee, Tokyo, Japan, 2005, pp. 137–142.

[4] Sasa, S., Yoshida, H., Ohashi, K., and Miyazaki, T., "Flight Test Overview of Ground to Stratosphere Flight Test Vehicle," *The Fifth Stratospheric Platform Systems Workshop Proceedings*, SPSW2005 Program Committee, Tokyo, Japan, 2005, pp. 123–128.

[5] Sasaki, Y., Eguchi, K., Kohno, T., and Maekawa, S., "Scenario for Development of the SPF Airship Technology Demonstrator," *The Fifth Stratospheric Platform Systems Workshop Proceedings*, SPSW2005 Program Committee, Tokyo, Japan, 2005, pp. 191–198.

[6] Maekawa, S., "On the Design Issue of a Stratospheric Platform Airship Structure," National Aerospace Laboratory of Japan, Rept. TM-772, May 2003.

[7] Federal Aviation Administration, "Airship Design Criteria," Federal Aviation Administration, Rept. P-8110-2 CHG 2, 1995.

[8] Khoury, G., and Gillett, J. (eds.), *Airship Technology*, Cambridge Univ. Press, Cambridge, England, U.K., 1999.

[9] Maekawa, S., and Saito, K., "The Effect of Ballonet Slosh on an Airship's Longitudinal Motion," *Transactions of the Japan Society for Aeronautical and Space Sciences*, Vol. 47, No. 155, May 2004.

[10] Abramson, H. N. (ed.), "The Dynamic Behavior of Liquids in Moving Containers," NASA SP-106, 1966.